

## Accepted Manuscript

Resonance analysis of a high temperature piezoelectric disc for sensitivity characterization

Prathamesh N. Bilgunde, Leonard J. Bond

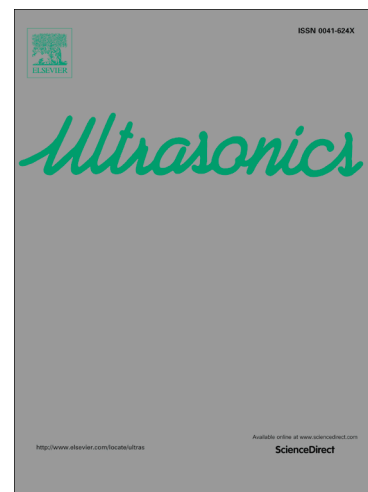
PII: S0041-624X(17)30902-2  
DOI: <https://doi.org/10.1016/j.ultras.2018.02.007>  
Reference: ULTRAS 5700

To appear in: *Ultrasonics*

Received Date: 29 October 2017  
Revised Date: 5 February 2018  
Accepted Date: 7 February 2018

Please cite this article as: P.N. Bilgunde, L.J. Bond, Resonance analysis of a high temperature piezoelectric disc for sensitivity characterization, *Ultrasonics* (2018), doi: <https://doi.org/10.1016/j.ultras.2018.02.007>

This is a PDF file of an unedited manuscript that has been accepted for publication. As a service to our customers we are providing this early version of the manuscript. The manuscript will undergo copyediting, typesetting, and review of the resulting proof before it is published in its final form. Please note that during the production process errors may be discovered which could affect the content, and all legal disclaimers that apply to the journal pertain.



# Resonance analysis of a high temperature piezoelectric disc for sensitivity characterization

Prathamesh N. Bilgunde<sup>1</sup> and Leonard J. Bond<sup>1, 2, a)</sup>

<sup>1</sup>Department of Aerospace Engineering, Iowa State University

<sup>2</sup>Center for NDE, Iowa State University, 1915 Scholl Road, Ames, IA-50011

<sup>a)</sup> Corresponding author: bondlj@iastate.edu

## Abstract:

Ultrasonic transducers for high temperature (200°C+) applications are a key enabling technology for advanced nuclear power systems and in a range of chemical and petro-chemical industries. Design, fabrication and optimization of such transducers using piezoelectric materials remains a challenge. In this work, experimental data-based analysis is performed to investigate the fundamental causal factors for the resonance characteristics of a piezoelectric disc at elevated temperatures. The effect of all ten temperature-dependent piezoelectric constants ( $\epsilon_{33}$ ,  $\epsilon_{11}$ ,  $d_{33}$ ,  $d_{31}$ ,  $d_{15}$ ,  $s_{11}$ ,  $s_{12}$ ,  $s_{13}$ ,  $s_{33}$ ,  $s_{44}$ ) is studied numerically on both the radial and thickness mode resonances of a piezoelectric disc. A sensitivity index is defined to quantify the effect of each of the temperature-dependent coefficients on the resonance modes of the modified lead zirconium titanate disc. The temperature dependence of  $s_{33}$  showed highest sensitivity towards the thickness resonance mode followed by  $\epsilon_{33}$ ,  $s_{11}$ ,  $s_{13}$ ,  $s_{12}$ ,  $d_{31}$ ,  $d_{33}$ ,  $s_{44}$ ,  $\epsilon_{11}$ , and  $d_{15}$  in the decreasing order of the sensitivity index. For radial resonance modes, the temperature dependence of  $\epsilon_{33}$  showed highest sensitivity index followed by  $s_{11}$ ,  $s_{12}$  and  $d_{31}$  coefficient. This numerical study demonstrates that the magnitude of  $d_{33}$  is not the sole factor that affects the resonance characteristics of the piezoelectric disc at high temperatures. It appears that there exists a complex interplay between various temperature dependent piezoelectric coefficients that causes reduction in the thickness mode resonance frequencies which is found to be agreement in with the experimental data at an elevated temperature.

*Keywords: piezoelectric; transducer; ultrasonics; high temperature; finite element*

## 1. Introduction

Generation IV fast nuclear reactor designs are being developed to support sustainable development, economic competitiveness, and improved safety [1]. Providing in-service inspection and repair (ISI&R) is a key enabling technology and presents major technical challenges which must be addressed to ensure safety of liquid sodium cooled fast reactors [2].

31 The technology has been of interest for several decades with US activity dating back to the early 1970s. A number  
32 of other countries (especially India, Japan, France, and Great Britain) have built and operated fast, metal-cooled  
33 reactors and supporting diagnostic instrumentation for in-service inspections [3]. Previous experimental studies  
34 have shown that design and fabrication of transducers that can simply survive in a reactor or other high temperature  
35 environment is challenging and that the signal strength reduces significantly for piezoelectric based ultrasonic  
36 transducers from room temperature to operating in liquid sodium at a hot stand-by temperature of  $\sim 260^{\circ}\text{C}$  [3-4].  
37 Studies that address aspects of high temperature transducer performance continue to be performed [5-9]. Recently,  
38 Searfass et al. [5] and Amini et al. [6] have quantified the ultrasonic signal strength of high temperature piezoelectric  
39 transducers for non-destructive evaluation (NDE) up to  $800^{\circ}\text{C}$ . Baptista et al. [7] utilized the insights from  
40 measuring the electrical impedance of the piezoelectric sensor as a method for experimental quantification of the  
41 temperature effect. Lately, Enciu et al. [8] and Haidar et al. [9] also investigated the temperature dependence of the  
42 piezoelectric material for the structural health monitoring (SHM) applications up to  $250^{\circ}\text{C}$ .

43 The resonance characteristics of such ultrasonic transducers determines the defect detection capability and mainly  
44 depends upon the piezoelectric effect. This effect is described by temperature dependent piezoelectric material  
45 coefficients [10] which in turn depend upon extrinsic and intrinsic contributions from the ceramic itself [11].

46 The temperature dependence of these various material coefficients of the different piezoelectric ceramics have been  
47 studied experimentally by many authors [e.g.12-15]. Sabat et al. [13] quantified the temperature dependence for  
48 modified Lead Zirconate Titanate ceramic (PZT-5A) as a function of temperature up to  $195^{\circ}\text{C}$ . Recently, Qaisar et  
49 al. [14] investigated the temperature dependence of  $d_{33}$  as a function of aging time, applied stress and temperature  
50 for soft and hard PZT-5A. Tang et al. [15] also reported the temperature dependence of a set of self-consistent full  
51 matrix material constants for PZT ceramics using a single sample for the resonance ultrasound spectroscopy method.  
52 This work also emphasized on the need for cost-efficient computer simulations to predict performance of high  
53 temperature electromechanical sensors. However, to address this need, it is necessary to describe the cause-effect  
54 relationships between the temperature dependent piezoelectric material coefficients and the resonance characteristics  
55 of an ultrasonic transducer.

56 It has been shown in previous experimental data [13] that each of the ten piezoelectric material parameters vary  
57 by different percentages at higher temperatures as compared to their baseline value at room temperature. Roy et al.

58 [16] modeled seven out of ten-independent piezoelectric material coefficients for temperature up 70°C to simulate  
 59 the temperature effect on a resulting ultrasonic signal. However, the contribution of each material coefficient to the  
 60 ultrasonic signal was not quantified. Recently, Janapati et al. [17] and Perez et al. [18] performed numerical  
 61 sensitivity studies to seek to understand the contribution of each coefficient to performance. This work involved  
 62 varying selected material parameters by a fixed percentage. The limitation of such a sensitivity analysis approach is  
 63 that a fixed percentage variation does not adequately capture the physical phenomenon in ceramics which is  
 64 affecting each of the piezoelectric material parameters at high temperatures.

65 The effects of this physical phenomenon on the resonance frequencies of a piezoelectric disc need to be  
 66 fundamentally quantified to enable adequate design and performance prediction for robust high temperature  
 67 transducers for use in NDE and SHM. The primary objective of this study is thus to quantify the contribution of each  
 68 piezoelectric material coefficient to the resonance modes of a disc as the temperature is increased. Hence, an  
 69 experimental data-based methodology is presented by solving an axisymmetric problem in a finite element (FE)  
 70 model. The changes to the thickness and radial modes in the resonance spectrum due to a temperature dependent  
 71 material parameter are quantified by a sensitivity index. Lastly, the change in the resonance spectra due to a  
 72 combined effect of varying all ten material parameters is compared with the experimental observations.

73 In the present study, section 2 describes the theory and relevant assumptions regarding piezoelectricity. Section 3  
 74 describes the methodology including the governing equations and discretization for the FE based model. Sections 4  
 75 and 5 present the simulation results and the discussion of the contribution for each material coefficient to the  
 76 resonance modes. Section 6 presents conclusions based on the experimental data-based methodology.

## 77 2. Theory

78 The assumptions for the current work are described by the theory of piezoelectricity at a corresponding temperature.  
 79 The fundamental equations can be obtained using Gibbs potentials, which is given by [7]

$$80 \quad S_i = s_{ij}^{E,H,\theta} T_j + d_{mi}^{H,\theta} E_m + d_{mi}^{H,\theta} H_m + \alpha_i^{E,H} d\theta \quad (1)$$

$$81 \quad D_m = d_{mi}^{H,\theta} T_i + \varepsilon_{mk}^{T,H,\theta} E_k + m_{mk}^{T,\theta} H_k + p_m^{T,H} d\theta \quad (2)$$

82 where  $S_i$  is the Cauchy's total mechanical strain tensor,  $D$  is the electric displacement tensor,  $\epsilon_{mk}^{T,H,\theta}$  is the absolute  
 83 permittivity and  $s_{ij}^{E,H,\theta}$  is the elastic compliance coefficient at a constant mechanical stress  $T$ , constant electric  
 84 field  $E$ , constant magnetic field  $H$  and a corresponding temperature  $\theta$ . The  $d_{mi}$  is the piezoelectric charge coefficient.  
 85 The thermal expansion coefficient and pyroelectric constant are given by  $\alpha$  and  $p$  respectively. The magneto-  
 86 dielectric coefficient is given by  $m$ . Phase velocity of elastic waves for a piezoelectric ceramic is significantly less  
 87 than that for the electromagnetic waves. This implies a time derivative of magnetic field  $H \approx 0$  indicating absence  
 88 of magnetization effects and presence of a quasi-static field. Thus, magneto-dielectric coupling from equations (1-2)  
 89 can be ignored at a corresponding high temperature  $\theta$ . In the current work, the temperature difference  $d\theta$  is assumed  
 90 to be small representing a gradual increase in the temperature of an ultrasonic transducer. Thus, for a quasi-thermal  
 91 change in the piezoelectric material, the thermal expansion and pyroelectric effect can be ignored. This reduces  
 92 equation (1-2) to a strain charge form of the piezoelectric effect at a corresponding temperature  $\theta$  is given by

$$93 \quad S_i = s_{ij}^{E,\theta} T_j + d_{mi}^{\theta} E_m \quad (3)$$

$$94 \quad D_m = d_{mi}^{\theta} T_i + \epsilon_{mk}^{T,\theta} E_k \quad (4)$$

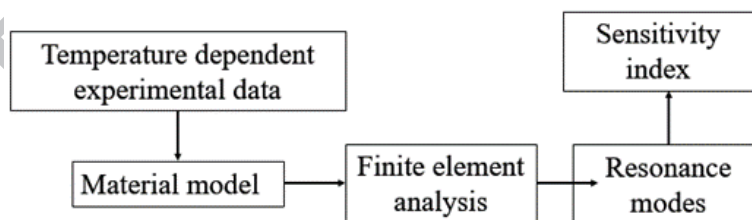
95 Ferroelectric ceramics such as soft-lead zirconium titanate ( $\text{Pb}[\text{Zr}_x\text{Ti}_{1-x}]\text{O}_3$ ), which are widely used in the ultrasonic  
 96 transducers, exhibit both intrinsic and extrinsic contributions to the piezoelectric effect [10-11] shown in equation  
 97 (3) and (4). This effect is dependent on the elastic, dielectric, and piezoelectric material coefficients [10]. Equations  
 98 (3-4) can also be represented in the matrix form as

$$99 \quad \begin{bmatrix} S1 \\ S2 \\ S3 \\ S4 \\ S5 \\ S6 \\ D1 \\ D2 \\ D3 \end{bmatrix} = \begin{bmatrix} s_{11}^E & s_{12}^E & s_{13}^E & 0 & 0 & 0 & 0 & 0 & d_{31} \\ s_{12}^E & s_{11}^E & s_{13}^E & 0 & 0 & 0 & 0 & 0 & d_{31} \\ s_{13}^E & s_{13}^E & s_{33}^E & 0 & 0 & 0 & 0 & 0 & d_{33} \\ 0 & 0 & 0 & s_{44}^E & 0 & 0 & 0 & d_{15} & 0 \\ 0 & 0 & 0 & 0 & s_{44}^E & 0 & d_{15} & 0 & 0 \\ 0 & 0 & 0 & 0 & 0 & 2(s_{11}^E - s_{12}^E) & 0 & 0 & 0 \\ 0 & 0 & 0 & 0 & d_{15} & 0 & \epsilon_{11}^T & 0 & 0 \\ 0 & 0 & 0 & d_{15} & 0 & 0 & 0 & \epsilon_{11}^T & 0 \\ d_{31} & d_{31} & d_{33} & 0 & 0 & 0 & 0 & 0 & \epsilon_{33}^T \end{bmatrix} \begin{bmatrix} T_1 \\ T_2 \\ T_3 \\ T_4 \\ T_5 \\ T_6 \\ E_1 \\ E_2 \\ E_3 \end{bmatrix} \quad (5)$$

100 Due to the crystal symmetry and polarization of Pb [Zr<sub>x</sub>Ti<sub>1-x</sub>]O<sub>3</sub> (PZT-5A), the complete material matrix reduces to  
 101 the five elastic ( $s_{11}, s_{12}, s_{13}, s_{33}, s_{44}$ ), three piezoelectric ( $d_{15}, d_{33}, d_{31}$ ) and two dielectric coefficients ( $\epsilon_{11}, \epsilon_{33}$ ) as shown  
 102 in equation (5). Hence, the piezoelectric effect given by equation (5) essentially represents the physical phenomenon  
 103 that occurs in the PZT-5A as the temperature is increased. Thus, the temperature dependent data [13] for these ten  
 104 mutually independent coefficients from equation (5) describe the linear theory for the piezoelectric effect under the  
 105 assumptions that—(a) the piezoelectric material remains linearly elastic, and (b) the applied electric field and  
 106 mechanical stress are small, which thus implies that this theory is not applicable for large deformations of the  
 107 piezoelectric material. This assumption is valid for the low-power piezoelectric based ultrasonic transducers which  
 108 are used in linear ultrasonic measurements employed in SHM and NDE.

### 109 3. Method

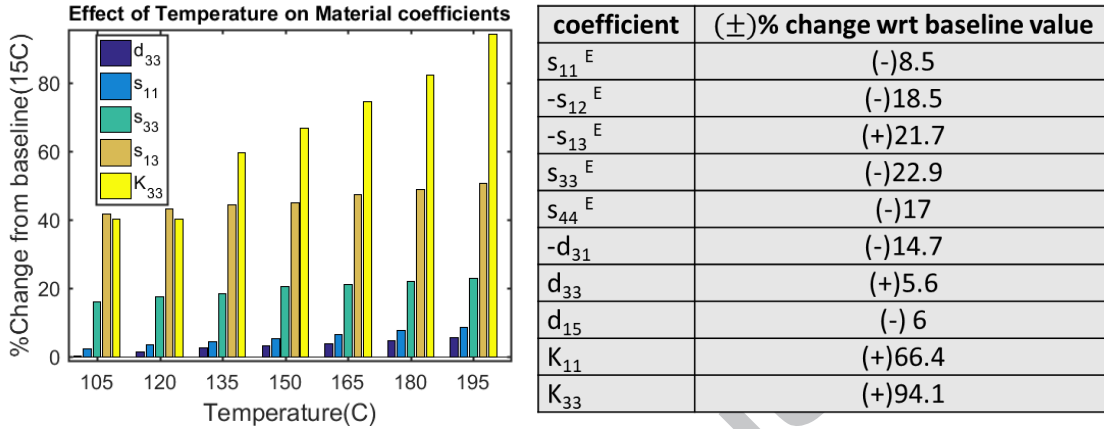
110 To develop an understanding of sensitivity for each temperature dependent material coefficient from equation (5), a  
 111 methodology is proposed as shown in Fig.1. A material model as described in equation (5) is formed using the  
 112 temperature dependent experimental data for elastic compliance ( $s_{ij}$ ), piezoelectric charge coefficient ( $d_{mi}$ ) and  
 113 dielectric permittivity ( $\epsilon_{mk}$ ). The material model forms the input parameters for a frequency domain finite element  
 114 (FDFE) analysis. The FDFE approach is basically a pseudo-static problem that requires no time stepping [19]. The  
 115 current FDFE model utilizes the temperature dependent experimental data for the soft, PZT-5A (Pb [Zr<sub>x</sub>Ti<sub>1-x</sub>]O<sub>3</sub>)  
 116 material given by Sabat et al. [13] which is in the morphotropic phase boundary (MPB) condition ( $x=0.52$ ). This  
 117 phase boundary condition increases the piezoelectric response of the material.



118  
119 Figure 1 Methodology for the sensitivity characterization

120 The experimental data as a function of temperature for piezoelectric material coefficients is shown in Fig.2. The  
 121 magnitude of each material coefficient at 195°C is compared with the percentage change from a baseline value at 15°  
 122 C. Each material coefficient varies by a different percentage when compared to the baseline value as shown in

123 Fig.2. Zhang and Yu (2011) [20] reviewed material properties of high temperature piezoelectric materials. The  
 124 variation in these piezoelectric material properties is dependent on the composition, dopants, grain size, internal  
 125 defects and the magnitude of temperature increase from the room temperature [13].



126

127

Figure 2 Temperature dependent piezoelectric material coefficients [13]

128

129

130

131

132

133

134

135

In this work, for the case of soft PZT-5A, the dielectric constant  $K_{33}$  in the poling direction demonstrates a maximum (94%) change as compared to the baseline value followed by  $K_{11}$  (66%) as shown Fig.2. The weakening of the ionic movements in the piezoelectric crystal raises the ionic polarizability [13] which increase the magnitude of dielectric constants  $K_{11}$ , and  $K_{33}$  with the temperature. The variation in the elastic coefficients of soft  $\text{Pb}[\text{Zr}_x\text{Ti}_{1-x}]\text{O}_3$  (PZT-5A) with increasing temperature could be due to the first order phase transition in the crystal structure [13]. Moreover, the variation in piezoelectric charge coefficients ( $d_{15}$ ,  $d_{33}$ ,  $d_{31}$ ) can be attributed to the increased domain wall motion with the temperature increase, which changes the activation energy required and hence, the extrinsic piezoelectric response [13].

136

137

138

139

In the current FDFE modeling approach, electrical admittance [7-9] is evaluated to quantify this temperature dependence of intrinsic and extrinsic contributions to the piezoelectric effect. The change in the admittance spectrum due to a material parameter change is quantified by an index to understand the sensitivity of resonance characteristics to a single temperature dependent material coefficient.

### 140 3.1 Finite element model

141

142

A physics-based model is formulated in COMSOL™ [21] using a Lagrangian formulation. An axisymmetric problem with quadratic shape function is solved for the geometric configuration of a piezoelectric disc as shown in

143 Fig.3. In the case of an axisymmetric problem, the elastic, piezoelectric and dielectric coefficients in the material  
 144 matrix shown in equation (5) reduce to

$$145 \quad s^E = \begin{bmatrix} s_{11}^E & s_{12}^E & s_{13}^E & 0 \\ s_{12}^E & s_{11}^E & s_{13}^E & 0 \\ s_{13}^E & s_{13}^E & s_{33}^E & 0 \\ 0 & 0 & 0 & s_{44}^E \end{bmatrix} \quad (6)$$

$$146 \quad d = \begin{bmatrix} 0 & 0 & 0 & d_{15} \\ d_{31} & d_{31} & d_{33} & 0 \end{bmatrix}, \quad \varepsilon^T = \begin{bmatrix} \varepsilon_{11}^T & 0 \\ 0 & \varepsilon_{33}^T \end{bmatrix} \quad (7)$$

147 The mechanical strain  $S_i$  is given by

$$148 \quad S_1 = s_{11}^E T_1 + s_{12}^E T_2 + s_{13}^E T_3 + d_{31} E_3 \quad (8)$$

$$149 \quad S_2 = s_{12}^E T_1 + s_{11}^E T_2 + s_{13}^E T_3 + d_{31} E_3 \quad (9)$$

$$150 \quad S_3 = s_{13}^E T_1 + s_{13}^E T_2 + s_{33}^E T_3 + d_{33} E_3 \quad (10)$$

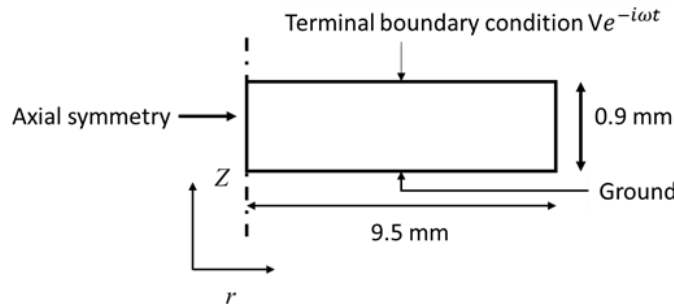
$$151 \quad S_4 = s_{44}^E T_4 + d_{15} E_2 \quad (11)$$

152 The electric displacements  $D_m$  from equation (4) and (5) reduce to

$$153 \quad D_2 = d_{15} T_4 + \varepsilon_{11}^T E_2 \quad (12)$$

$$154 \quad D_3 = d_{31} T_1 + d_{31} T_2 + d_{33} T_3 + \varepsilon_{33}^T E_3 \quad (13)$$

155 The baseline material parameters (at 15°C) for the current study are given in Table I. The poling direction of the  
 156 piezoelectric disc is aligned with z direction of the model in the cylindrical coordinate system, as shown in Fig. 3.



157  
 158 Figure 3 Geometric configuration of the problem

159 The FDFE formulation represents a time harmonic nature for the mechanical displacement  $u=u(r,z)e^{i\omega t}$  and stress  
 160  $\sigma=\sigma(r,z)e^{i\omega t}$  in the cylindrical coordinate space  $(r,\phi,z)$ . Here, the  $e^{i\omega t}$  term describes this harmonic nature of the

161 mechanical displacement and stress. The equation for linear momentum balance in the frequency domain is thus  
 162 given by

$$163 \quad \rho \omega^2 u + \nabla \cdot \sigma = F_v e^{i\phi} \quad (14)$$

164 where  $\rho$  is the assigned material density,  $\omega$  is the angular frequency, and  $F_v$  is the body force. The boundaries  $z=0$ ,  
 165  $z=0.9$  mm and  $r=9.5$ mm shown in Fig.3 are kept traction free implying  $\sigma_{31}=\sigma_{33}=\sigma_{11}=0$ .

**Table I-Baseline (15°C) material parameters for PZT-5A**

$s_{11}^E$	$16.4 \times 10^{-12}$ (1/Pa)
$s_{12}^E$	$-5.74 \times 10^{-12}$ (1/Pa)
$s_{13}^E$	$-7.22 \times 10^{-12}$ (1/Pa)
$s_{33}^E$	$18.8 \times 10^{-12}$ (1/Pa)
$s_{44}^E$	$47.5 \times 10^{-12}$ (1/Pa)
$d_{31}$	$-1.71 \times 10^{-10}$ (C/N)
$d_{33}$	$3.74 \times 10^{-10}$ (C/N)
$d_{15}$	$5.85 \times 10^{-10}$ (C/N)
$K_{11}$ (relative permittivity)	1730
$K_{33}$ (relative permittivity)	1700
Rayleigh damping coeff. ( $\alpha$ )	$7.3 \times 10^4$ (1/s)
Rayleigh damping coeff. ( $\beta$ )	$5.48 \times 10^{-9}$ (s)
Density ( $\rho$ )	7750 (kg/m <sup>3</sup> )

166  
 167 Mechanical damping in the piezoelectric material is modelled using the Rayleigh damping model [22] which is  
 168 given as

$$169 \quad [C_{uu}] = \alpha [M_{uu}] + \beta [K_{uu}] \quad (15)$$

170 where  $C_{uu}$  is the damping matrix,  $M_{uu}$  is the mass matrix and  $K_{uu}$  is the stiffness matrix assembled at the global level  
 171 in the FE model. The Rayleigh damping coefficient for mass and stiffness matrix are denoted by  $\alpha$  and  $\beta$   
 172 respectively. For the phenomenological modeling of attenuation due to damping, the Rayleigh damping coefficients  
 173 are assumed to be constant [21]. Equation (14) thus becomes [21]

$$174 \quad -\rho \omega^2 u + i\omega \alpha_{dm} \rho u = \nabla \cdot (\sigma + i\omega \beta_{dk} c_E : \varepsilon_{el}) + F_v e^{i\phi} \quad (16)$$

175 For the piezoelectric media, a quasi-static field is assumed as stated in previous section. Thus, the electric field  $E$  is  
 176 related to the scalar electric potential  $V$  as given by

$$177 \quad E = -\nabla V \quad (17)$$

178 A unit magnitude voltage is applied to the boundary  $z=0.9$  mm by using a terminal boundary condition assigned to  
 179 PZT-5A as shown in Fig.3. The electric current in the piezoelectric domain  $\partial^D \Omega_{piezo}$  is given by [21]

$$180 \quad \int_{\partial^D \Omega_{piezo}} D \cdot n = Q_0, \frac{dQ_0}{dt} = I_{cir} \quad (18)$$

181 Electrical admittance is given by  $Y = G + jB$  where  $G$  is the real part of admittance known as conductance whereas  $B$   
 182 is the imaginary part known as susceptance. In the present sensitivity study, the susceptance spectrum is plotted to  
 183 quantify change in the resonance spectrum due to each material coefficient. The element size for spatial  
 184 discretization is determined using the shear wave speed value  $c$  (3895 m/s) in the piezoelectric domain at the  
 185 frequency  $f_0$  (2.25MHz). The number of elements per wavelength  $N$  is set equal to 10 by performing the numerical  
 186 convergence study. Maximum element size  $h_{max}$  is thus given as

$$187 \quad h_{max} = \frac{c}{f_0 N} \quad (19)$$

188 For this case, a quadrilateral element of size 0.02mm is used for mapped meshing technique of the domain  $\Omega_{piezo}$   
 189 shown in Fig.3. The sensitivity of the temperature dependent material coefficient in terms of impact on the  
 190 resonance spectrum is characterized using the metric indices. One such metric is the root mean square deviation  
 191 (RMSD) which is given by

$$192 \quad RMSD = \sum_{n=\omega_l}^{n=\omega_f} \sqrt{\frac{[Z_{E,B}(n) - Z_{E,T}(n)]^2}{Z_{E,B}^2(n)}} \quad (20)$$

193 where  $\omega_l$  is the start frequency and  $\omega_f$  is the final frequency.  $Z_{E,B}$  is the baseline electrical admittance value at 15C  
 194 while  $Z_{E,T}$  is the admittance signature at the corresponding temperature  $T$  simulated at frequency  $n$ .

195

## 4. Results

196

197

198

199

A stationary, Multifrontal Massively Parallel Sparse (MUMPS) direct solver is used for computation which is the default solver setting for frequency domain studies in COMSOL™ [20]. The model is solved for 193,695 degrees of freedom. A frequency sweep is performed from 10 kHz to 4.5 MHz in steps of 10 kHz. This increases the number of sample points in the admittance spectra and hence the resolution of the computed resonance spectrum.

200

## 4.1 Validation of model data with the reference experimental data:

201

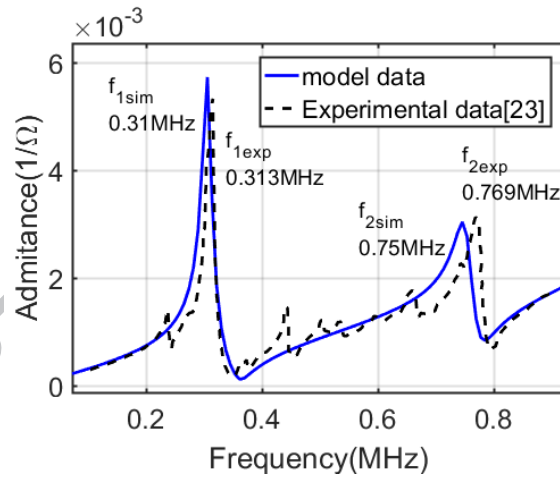
202

203

204

205

The baseline FE model is compared with the room temperature experimental data [23] before performing the sensitivity study. Good agreement with the experimental and model data is obtained at room temperature for the resonant and anti-resonant frequencies as shown in Fig.4. The percentage difference for the resonance frequencies  $f_1$  and  $f_2$  are less than 3% between the model and experimental data. The magnitude of the admittance corresponding to the resonant frequency from model data is also in good agreement with the experimental data shown in Fig. 4.



206

207

208

Figure 4 Comparison of model data (blue line) and experimental data [23] (black dashed line) for the electrical admittance of PZT-5A at room temperature.

209

## 4.2 Radial resonance mode

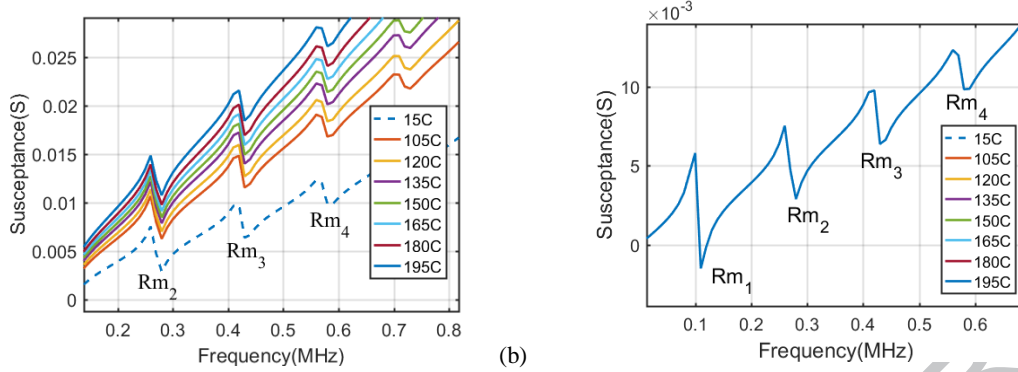
210

211

212

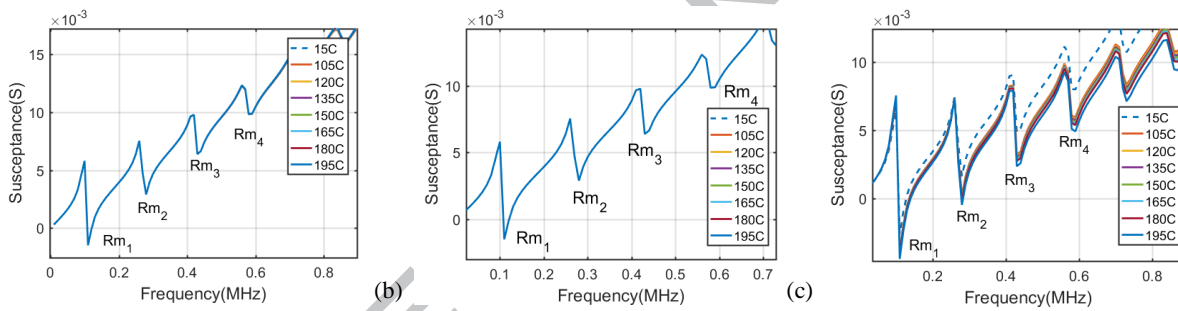
213

The magnitude of  $K_{33}$  increases by 94% and  $K_{11}$  increases by 66% as the temperature increases from 15 to 195°C [13]. This increase in  $K_{33}$  increases the magnitude of susceptance as shown in Fig.5(a). However, the temperature dependent variation in dielectric constant in the radial direction  $K_{11}$  does not appear to affect the radial resonance mode as shown by the data given in Fig.5(b).



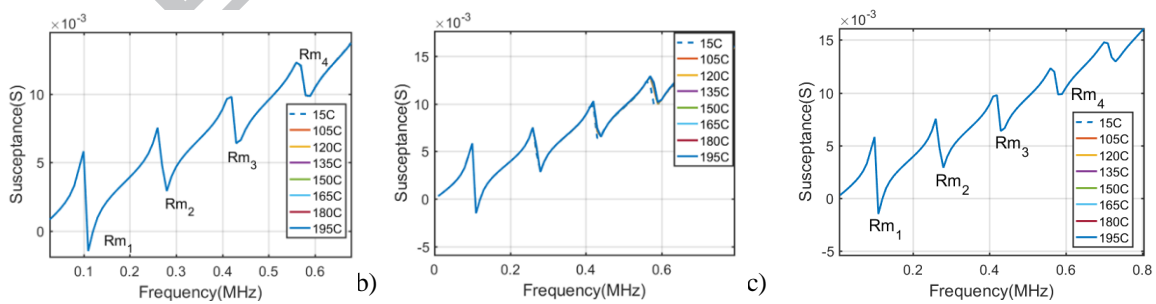
214 (a) (b)  
 215 Figure 5 Effect on radial resonance mode due to temperature dependent variation in (a)  $K_{33}$  (b)  $K_{11}$

216 Moreover, the temperature dependence of the piezoelectric charge coefficient  $d_{33}$  and  $d_{15}$  does not significantly  
 217 affect the radial resonance modes as shown by the data given in Fig. 6(a-b). However, with variation in  $d_{31}$  the  
 218 radial resonance mode increases marginally as shown in Fig.6(c) as the temperature is increased from 15 to 195°C.

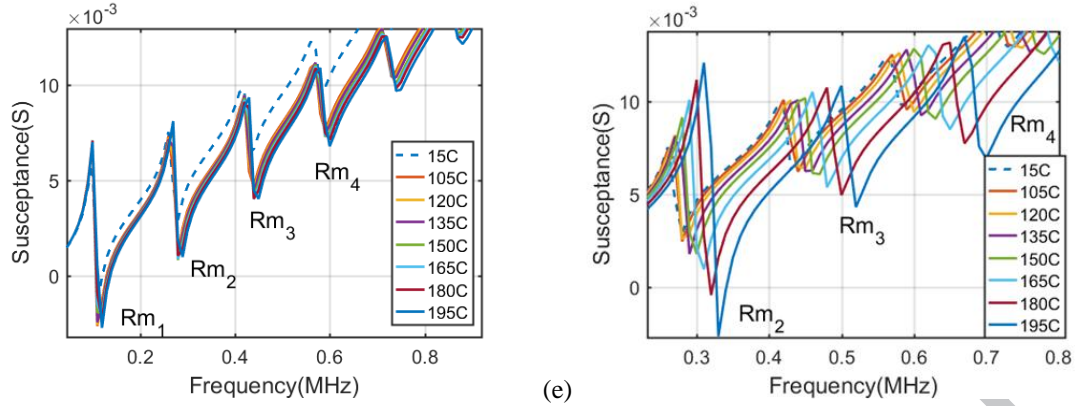


219 (a) (b) (c)  
 220 Figure 6 Effect on radial resonance mode due to temperature dependent variation in (a)  $d_{33}$  (b)  $d_{15}$  (c)  $d_{31}$

221 Interestingly, the radial resonance mode is also unaffected by the temperature dependence of the elastic compliance  
 222 coefficients  $s_{33}$ ,  $s_{13}$  and  $s_{44}$  as shown in Fig.7(a-c) which is discussed further in section 5.

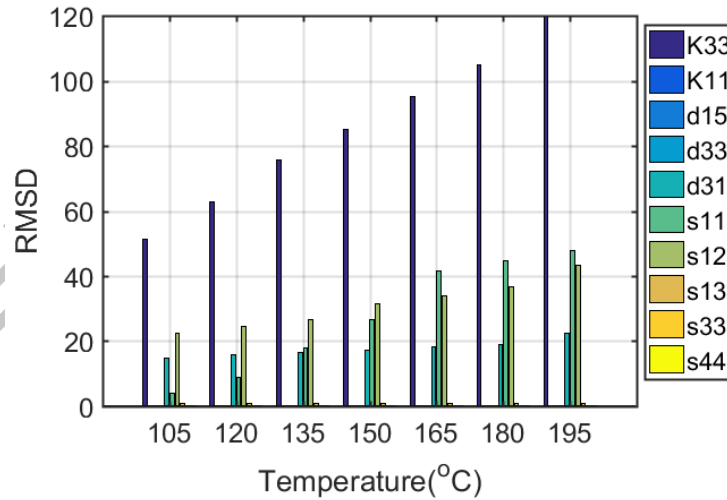


223 (a) (b) (c)



224 (d) (e)  
 225 Figure 7 Effect on radial resonance mode due to temperature dependent variation in a)  $s_{33}$  b)  $s_{13}$  c)  $s_{44}$  d)  $s_{12}$  e)  $s_{11}$

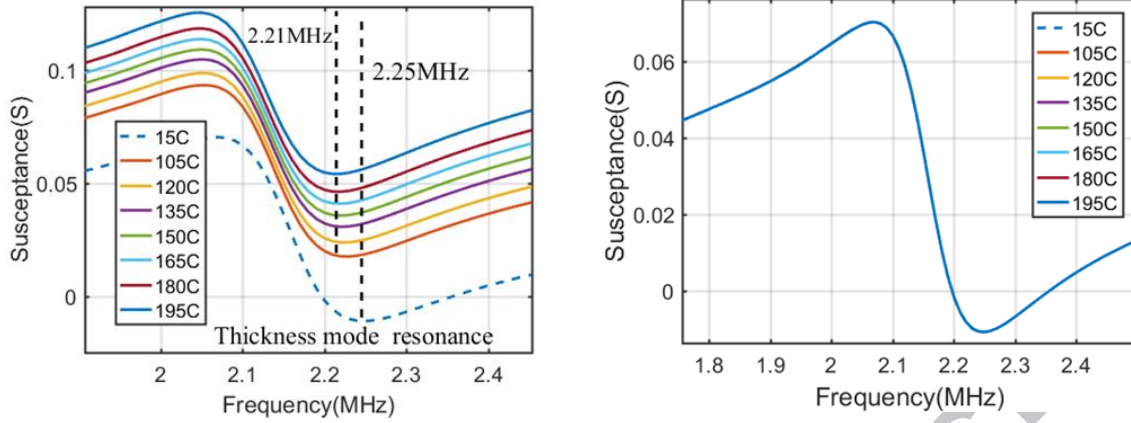
226 However, the temperature dependence of  $s_{12}$  over the temperature range from 15 to 195°C causes a marginal  
 227 increase in the radial resonance frequency as shown in Fig.7(d). Similarly, a decrease in  $s_{11}$  as a function of  
 228 temperature increases radial resonant frequency from 15 to 195°C as shown in Fig.7(e). These temperature  
 229 dependent changes are further quantified using the RMSD based index as shown in Fig.8. It can be seen that the  
 230 temperature dependence of  $K_{33}$ (or  $\epsilon_{33}$ ) causes maximum sensitivity in terms of changes in the radial resonance mode  
 231 followed by  $s_{11}$ ,  $s_{12}$  and  $d_{31}$  at 195°C.



232  
 233 Figure 8 sensitivity index for radial resonance mode due to temperature dependent variation in the ten material coefficients

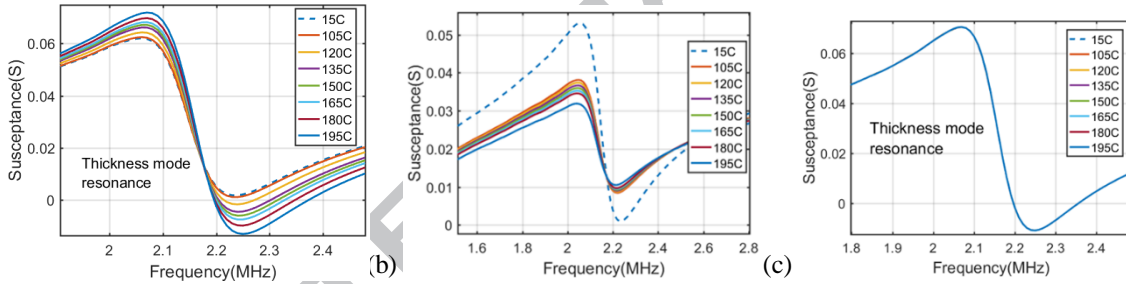
#### 234 4.3 Thickness resonance mode

235 The thickness resonance mode frequency reduces due to increase in  $K_{33}$  as a function of temperature as shown in  
 236 Fig.9(a). In a response which is similar to that for the radial mode frequency, the thickness mode frequency is also  
 237 unaffected by the 66% variation in temperature dependent  $K_{11}$  as shown in Fig.9(b).



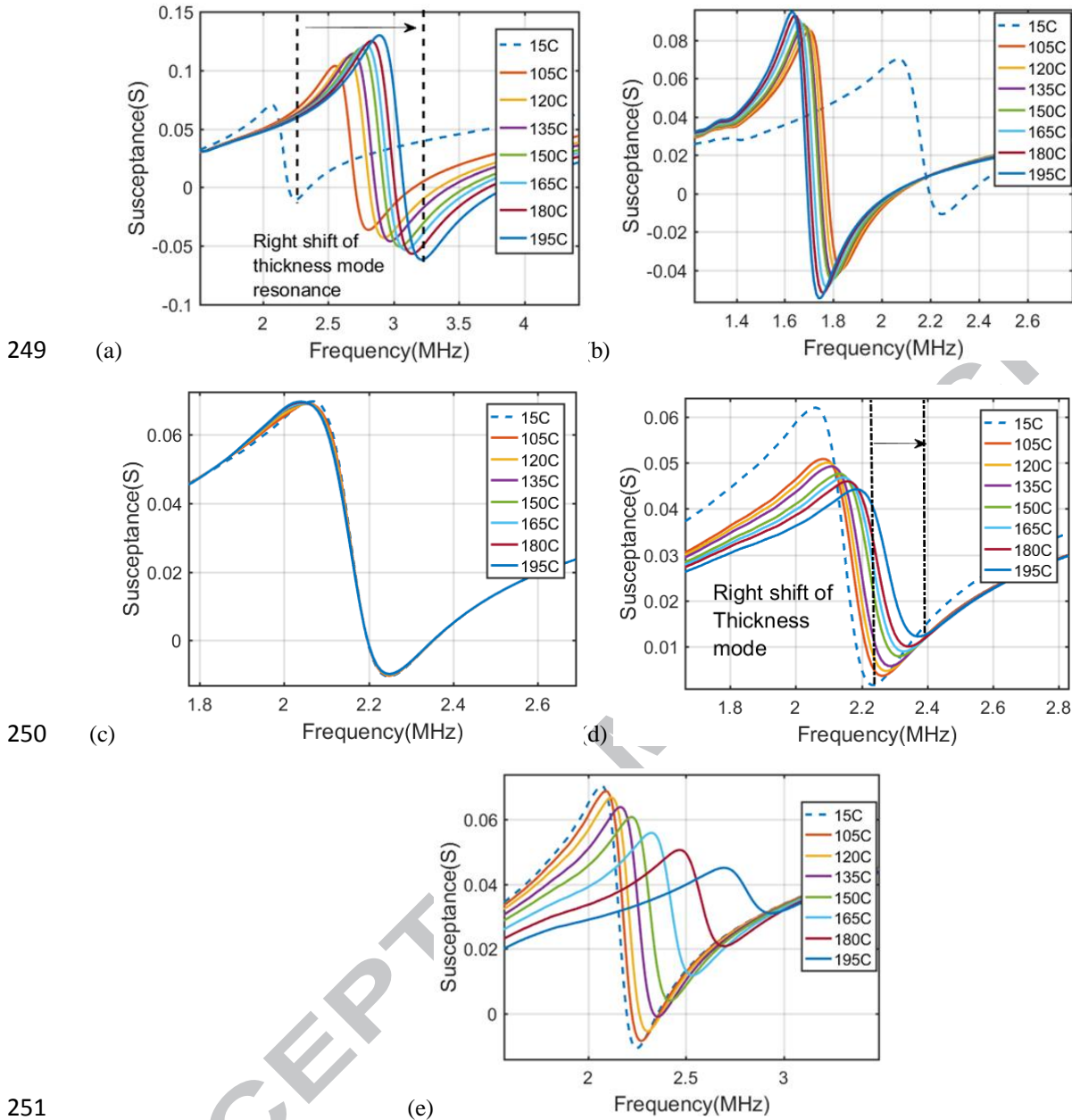
238  
239 Figure 9 Effect on thickness resonance mode due to temperature dependent variation (a)  $K_{33}$  (b)  $K_{11}$

240 However, for a 5.6% increase in  $d_{33}$ , the magnitude of the susceptance increases with temperature along with a  
241 marginal change in the resonance frequency as shown in Fig.10(a). The magnitude of the susceptance decreases for  
242 the variation in  $d_{31}$  in the temperature range 15 to 195°C as shown in Fig.10(b). The thickness resonance mode is  
243 completely unaffected by temperature with changes in  $d_{15}$  as shown in Fig.10(c).



244 (a) (b) (c)  
245 Figure 10 Effect on thickness resonance mode due to temperature dependent variation (a)  $d_{33}$  (b)  $d_{31}$  (c)  $d_{15}$

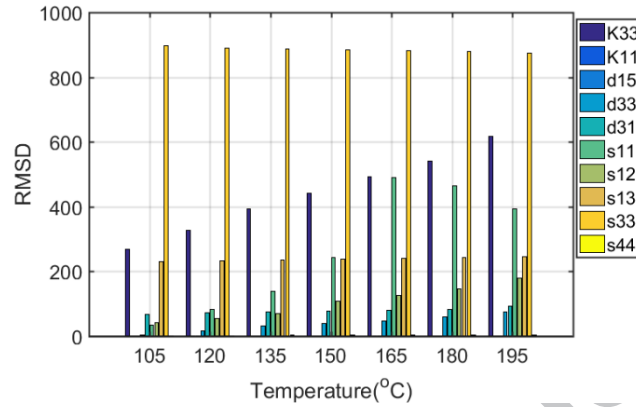
246 The reduction in the elastic compliance coefficient  $s_{33}$  in the thickness direction increases thickness resonance  
247 frequency causing a shift to a higher frequency in the spectrum as shown in Fig.11(a). This also implies that there is  
248 an increase in stiffness of the disc due to a reduction of  $s_{33}$ , as a function of temperature.



251  
252 Figure 11 Effect on thickness resonance mode due to temperature dependent variation (a) $s_{33}$  (b) $s_{13}$  (c) $s_{44}$  (d) $s_{12}$  (e) $s_{11}$

253 However, a variation in magnitude of  $s_{13}$  from 15 to 195°C causes a reduction in the resonance frequency and an  
 254 increase in the magnitude of susceptance as shown in Fig.11(b). The thickness mode remains unaffected by a 17%  
 255 reduction in  $s_{44}$  as shown in Fig.11(c). The temperature dependent variation in  $s_{12}$  also increases the resonant  
 256 frequency as shown in Fig.11(d). However, the magnitude of the susceptance decreases with an increase in the  
 257 temperature. Similar characteristics are observed for the temperature dependence of  $s_{11}$  as shown in Fig.11(e). The  
 258 change in the resonance frequency as a function of temperature are further quantified using the RMSD based

259 sensitivity index as shown in Fig.12. It can be seen that  $s_{33}$  exhibits the highest sensitivity followed by  $K_{33}$ , and  $s_{11}$   
 260 and then followed by the remaining temperature dependent material coefficients.



261  
 262 Figure 12 sensitivity index for thickness resonance mode due to temperature dependent variation in the ten temperature  
 263 dependent material coefficients

#### 264 4.4 Combined effect of various temperature dependent material coefficients

265 In previous sub-sections, analysis for the effect of temperature dependent variation in each piezoelectric material  
 266 coefficient was performed. In physical piezoelectric based transducer, these piezoelectric material parameters vary  
 267 simultaneously as a function of temperature. In this section, this case is modelled by considering the temperature  
 268 dependent variation which occurs in all material parameters simultaneously. The combined effect due to temperature  
 269 dependent variation of all material coefficients causes an increase in the magnitude of the susceptance as shown in  
 270 Fig.13(a-b). The combined effect due to the temperature dependent variation of all material coefficients causes an  
 271 increase in the magnitude of the susceptance as shown in Fig.13(a-b). The observed shift in the resonance spectrum  
 272 is due to the temperature effect on the piezoelectric material which is consistent with the previous experimental  
 273 observations by Baptista et al. [7] and Enciu et al. [8]. The increase in the magnitude of the susceptance (imaginary  
 274 part of admittance) at the resonance frequency due to this combined effect is shown in Fig.13(b), and this is in  
 275 agreement with the experimental observations reported by Haider et al. [9].

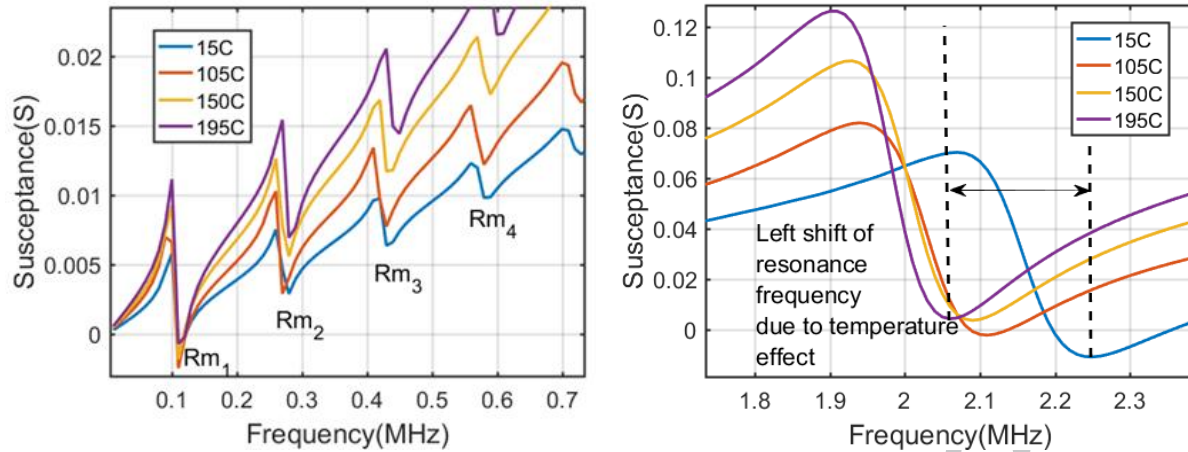


Figure 13 Combined temperature effect on (a) Radial resonance mode (b) Thickness resonance mode

276  
 277  
 278 This temperature dependent change in magnitude and the resonant frequency is quantified using the RMSD based  
 279 index as shown in Fig.14. The RMSD based index increases from 320 at 105°C to 664 at 150°C and reaches up to  
 280 687 at 195°C indicating a non-linear change in the material coefficients of PZT-5A from 105 to 195°C due to the  
 281 physical phenomenon explained in section 3.

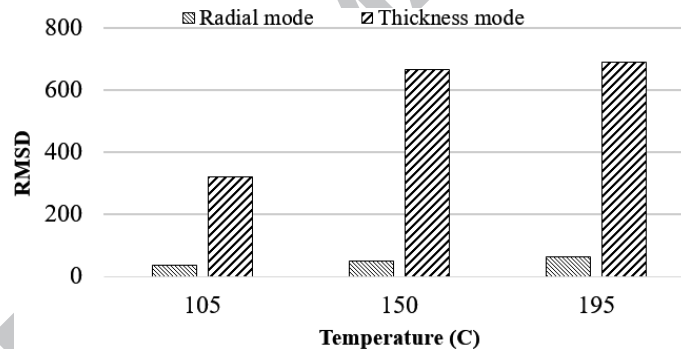


Figure 14 Sensitivity of the resonance modes for the combined temperature effect

## 5. Discussion

282  
 283  
 284  
 285 The sensitivity measured by the metric (RMSD) of each of the ten material coefficients for the temperature  
 286 dependent variation [13] as explained in section 3 was reported in previous section in Figs.8 and 12. Based on the  
 287 RMSD value, the thickness resonance mode is found to be more sensitive to the temperature change than the radial  
 288 modes due to the polarization of PZT-5A in the thickness direction. Here, Table II gives a summary of the  
 289 sensitivity value for the percentage change in the material coefficient value at 195°C compared to the baseline value  
 290 at 15°C. It is evident from Table II that the percentage change in the baseline value varies for different material  
 291 coefficients. This indicates that each material coefficient exhibits different absolute sensitivity to the temperature

292 change. For the case of PZT-5A, this sensitivity to the temperature change can be attributed to the (a) weakening of  
 293 ionic movements (b) first order phase transition and (c) domain wall motion in the piezoelectric material [13] as  
 294 explained previously in section 3. However, a higher percentage change from the baseline value does not ensure a  
 295 higher influence over the resulting changes in the resonance spectrum as seen from Table II. For example, the  
 296 relative permittivity  $K_{33}$  with a 94% increase, results in a RMSD value of 617, whereas a 66% increase in  $K_{11}$  results  
 297 in RMSD index of only 0.23. This counterintuitive phenomenon can be explained by contributions of a coefficient to  
 298 the piezoelectric effect. This piezoelectric effect was explained previously for the axisymmetric problem in terms of  
 299 mechanical strain and electric displacement given by equation (8) through (13). The parameter  $K_{33}$  contributes to the  
 300 magnitude of the electric displacement  $D_3$  whereas  $K_{11}$  contributes to  $D_2$ . The coefficient  $s_{33}^E$  contributes to the  
 301 mechanical strain  $S_3$ . Similarly,  $s_{11}^E$ ,  $s_{12}^E$  contribute to  $S_1$  and  $S_2$  whereas  $s_{13}^E$  contributes to  $S_1$ ,  $S_2$  and  $S_3$  as  
 302 described in equations (8), (9) and (10). These contributions of  $s_{11}^E$ ,  $s_{12}^E$  and  $s_{13}^E$  to the mechanical strain in the  
 303 principal directions can potentially explain a higher RMSD value for a lower percentage change in their baseline  
 304 value as quantified in Table II.

**Table II Summary of % change and RMSD value at 195°C**

coefficient	(±)% change compared to the baseline value	RMSD
$s_{11}^E$	(-)8.5	393
$-s_{12}^E$	(-)18.5	179
$-s_{13}^E$	(+)21.7	245
$s_{33}^E$	(-)22.9	874
$s_{44}^E$	(-)17	4
$-d_{31}$	(-)14.7	92
$d_{33}$	(+)5.6	74.1
$d_{15}$	(-) 6	0.18
$K_{11}$	(+)66.4	0.23
$K_{33}$	(+)94.1	617

305  
 306 For the disc shape geometry,  $s_{44}^E$  does not drive a large change in the resonance spectrum of the PZT-5A. This is  
 307 evident from a RMSD value of 4 although the baseline value of  $s_{44}^E$  is reduced by 17% at 195°C. The piezoelectric  
 308 charge coefficient  $d_{15}$  has the lowest RMSD with a value of 0.18 followed by  $K_{11}$  with a value of 0.23. Both of these  
 309 coefficients contribute to electric displacement  $D_2$ . Mechanical strain  $S_4$  and  $D_2$  do not affect the magnitude of the

310 susceptance spectrum for a soft PZT-5A disc. The  $d_{33}$  coefficient exhibits an RMSD value of 74 for the 5.6%  
 311 increase in the baseline value. It contributes to  $D_3$  and  $S_3$  as described in equations (10) and (13). The parameter  $d_{31}$   
 312 which contributes  $D_3$ ,  $S_2$ , and  $S_1$  results in a RMSD value of 92 for a 14.7% increase in the baseline absolute value.

313 The changes in the resonance spectrum when all ten material coefficients are varied using the temperature  
 314 dependent experimental data [13] is reported in Fig.13(a-b) of Section 4.4. This combined temperature effect  
 315 exhibits a reduction in the thickness resonance frequency as shown in Fig.13(b) which also indicates RMSD value  
 316 of 687 as shown in Fig.14 and Table II. Evidently, this sensitivity metric is 8 times greater than the  $d_{33}$  RMSD value  
 317 of 74. As explained previously, this significant difference is due to the different sensitivity of the material  
 318 coefficients to the temperature change and their contribution to the mechanical strain and electric displacement.

## 319 6. Conclusions

320 A 2D axisymmetric FE model has been developed to investigate the effect of temperature dependent material  
 321 coefficients on the resonance modes of a piezoelectric disc. Initially, the model is validated with the literature  
 322 experimental data for PZT-5A at room temperature. The FE model is subsequently used to study thickness and  
 323 radial mode resonance modes for temperature effects on elastic, piezoelectric and dielectric material coefficients  
 324 using the reference experimental data. The temperature effect for all the material coefficients on the resonance  
 325 spectrum is quantified using a root mean square deviation (RMSD) based sensitivity index.

326 It is demonstrated that the sensitivity of resonance modes due to the temperature effects on the material  
 327 coefficients is dependent on the percentage change in the baseline value as well as the contribution of that  
 328 coefficient to the mechanical strain and electric displacement. For a soft PZT-5A disc, at 195°C,  $s_{33}^E$  demonstrate  
 329 the highest sensitivity value followed by  $K_{33}$ ,  $s_{11}^E$ ,  $s_{13}^E$ ,  $s_{12}^E$ ,  $d_{31}$ , and  $d_{33}$  in the order of high to low RMSD value.  
 330 Changes in  $d_{15}$ ,  $K_{11}$  and  $s_{44}^E$  exhibit minimal effect on the thickness resonance modes at 195°C. For radial  
 331 resonance modes, the temperature dependence of  $\epsilon_{33}$  showed highest sensitivity index followed by the  $s_{11}$ ,  $s_{12}$  and  
 332  $d_{31}$  coefficients.

333 When all the ten material coefficients are varied based on the temperature dependent experimental data, the  
 334 combined temperature effect results in the reduction of the thickness mode resonance frequency. This causes a  
 335 reduction in the resonant frequency which is consistent with the observations from experimental work on the

336 temperature effect for piezoelectric sensors. The combined effect results in a RMSD value of 687 which is 8 times  
337 the RMSD value for temperature dependent changes in  $d_{33}$  at 195°C. This demonstrates that the magnitude of  $d_{33}$  is  
338 not the sole factor that affects the resonance characteristics of the piezoelectric based ultrasonic transducers at high  
339 temperatures. It further appears that a complex interplay between material coefficients results in a reduction of  
340 thickness mode resonance frequency as the temperature is increased. This interplay was discussed in this work in  
341 terms of the contribution of each of the piezoelectric material coefficients to the mechanical strain and electric  
342 displacement. The simulation results also show that the current methodology, based on the temperature dependent  
343 experimental data has potential to be a useful tool to estimate the performance of high temperature piezoelectric  
344 based ultrasonic transducers. Particularly, for application in nuclear reactor, resonance analysis of radiation tolerant  
345 piezoelectric materials could also be performed using the current methodology for the temperature sensitivity  
346 characterization. Future work will focus on describing the complex interplay with an equation consisting of a  
347 weighted sum of ten piezoelectric material parameters to evaluate resonance sensitivity at a particular temperature.

#### 348 Acknowledgement

349 This work was supported by U.S. Department of Energy's office of Nuclear Energy under Nuclear Energy  
350 University Program (NEUP). The authors would like to acknowledge generous support from Prof. Sabat  
351 (Department of Physics, Royal Military College of Canada, Kingston, Ontario K7K 7B4, Canada) for sharing the  
352 experimental data on PZT-5A (EC-65). Authors are also grateful to Dr. Vamshi Krishna Chillara (Las Alamos  
353 National Laboratory, New Mexico, USA) for his suggestions and review of the manuscript.

#### 354 Declaration of interest

355 Authors have no conflict of interest.

#### 356 References

- 357 [1] OECD "Technology roadmap update for generation IV nuclear energy systems," OECD Nuclear Energy  
358 Agency for the Generation IV International Forum (2014). [https://www.gen-  
359 4.org/gif/upload/docs/application/pdf/2014-03/gif-tru2014.pdf](https://www.gen-4.org/gif/upload/docs/application/pdf/2014-03/gif-tru2014.pdf)

- 360 [2] Lubeigt, E., Mensah, S., Chaix, J. F., Rakotonarivo, S., and Gobillot, G. "Ultrasonic imaging in liquid  
361 sodium: Topological energy for damages detection." In *4th International Conference on Advancements in  
362 Nuclear Instrumentation Measurement Methods and their Applications (ANIMMA)*, 1-5, IEEE. (2015)
- 363 [3] Kažys, R. J., Voleišis, A., and Voleišienė, B. "High temperature ultrasonic transducers" *Ultragarsas*, **63**(2),  
364 7-17 (2008).
- 365 [4] Griffin, J. W., Peters, T. J., Posakony, G. J., Chien, H. T., Bond, L. J., Denslow, K. M., Sheen, S. H. and  
366 Raptis, P. "Under-Sodium viewing: a review of ultrasonic imaging technology for liquid metal fast  
367 reactors," PNNL-18292, Pacific Northwest National Laboratory, Richland, WA (2009).
- 368 [5] Searfass, C. T., Pheil, C., Sinding, K., Tittmann, B. R., Baba, A., and Agrawal, D. K., "Bismuth Titanate  
369 Fabricated by Spray-on Deposition and Microwave Sintering for High-Temperature Ultrasonic  
370 Transducers". *IEEE Transactions on Ultrasonics, Ferroelectrics, and Frequency Control*, **63**(1), 139-146.  
371 (2016).
- 372 [6] Amini, M. H., Sinclair, A. N., and Coyle, T. W. "A New High-Temperature Ultrasonic Transducer for  
373 Continuous Inspection" *IEEE Transactions on Ultrasonics, Ferroelectrics, and Frequency Control*, **63**(3),  
374 448-455 (2016).
- 375 [7] Baptista, F. G., Budoya, D. E., de Almeida, V. A., and Ulson, J. A. C. "An experimental study on the effect  
376 of temperature on piezoelectric sensors for impedance-based structural health monitoring" *Sensors*, **14**(1),  
377 1208-1227 (2014).
- 378 [8] Enciu, D., Ursu, I., and Toader, A. "New results concerning structural health monitoring technology  
379 qualification for transfer to space vehicles" *Structural Control and Health Monitoring*, **24**:e1992 (2017)  
380 <http://dx.doi.org/10.1002/stc.1992>
- 381 [9] Haider, M. F., Giurgiutiu, V., Lin, B., and Yu, L. "Irreversibility effects in piezoelectric wafer active  
382 sensors after exposure to high temperature" *Smart Mater. Struct.*, **26**(9), 095019 (2017).
- 383 [10] Randall, C. A., Kim, N., Kucera, J. P., Cao, W., and Shrout, T. R. "Intrinsic and extrinsic size effects in  
384 fine-grained morphotropic-phase-boundary lead zirconate titanate ceramics". *Journal of the American  
385 Ceramic Society*, **81**(3), 677-688 (1998).
- 386 [11] Haun, M. J., Furman, E., Jang, S. J., McKinstry, H. A., and Cross, L. E. "Thermodynamic theory of  
387 PbTiO<sub>3</sub>" *Journal of Applied Physics*, **62**(8), 3331-3338 (1987).

- 388 [12] Zhang, S., Alberta, E. F., Eitel, R. E., Randall, C. A., and Shrout, T. R. "Elastic, piezoelectric, and  
389 dielectric characterization of modified BiScO<sub>3</sub>-PbTiO<sub>3</sub> ceramics" *IEEE Transactions on Ultrasonics,  
390 Ferroelectrics, and Frequency Control*, **52**(11), 2131-2139 (2005).
- 391 [13] Sabat, R.G., Mukherjee, B. K., Ren, W., and Yang, G. "Temperature dependence of the complete material  
392 coefficients matrix of soft and hard doped piezoelectric lead zirconate titanate ceramics" *Journal of Applied  
393 Physics*, **101**(6), 064111 (2007).
- 394 [14] Qaisar, S. A., Comyn, T. P., and Bell, A. J. "Temperature Dependence of Domain Contributions as a  
395 Function of Ageing in Soft and Hard Lead Zirconate Titanate Piezoelectric Ceramics." *IEEE Transactions  
396 on Ultrasonics, Ferroelectrics, and Frequency Control*, **64**(6), 1023-1028 (2017).
- 397 [15] Tang, L., and Cao, W. "Temperature dependence of self-consistent full matrix material constants of lead  
398 zirconate titanate ceramics". *Applied Physics Letters*, **106**(5), 052902 (2015)
- 399 [16] Roy, S., Lonkar, K., Janapati, V., and Chang, F. K., "A novel physics-based temperature compensation  
400 model for structural health monitoring using ultrasonic guided waves" *Structural Health Monitoring*, **13**(3),  
401 321-342 (2014).
- 402 [17] Janapati, V., Kopsaftopoulos, F., Li, F., Lee, S. J., and Chang, F. K. "Damage detection sensitivity  
403 characterization of acousto-ultrasound-based structural health monitoring techniques" *Structural Health  
404 Monitoring*, **15**(2), 143-161 (2016).
- 405 [18] Pérez, N., Buiocchi, F., Brizzotti Andrade, M. A., and Adamowski, J. C. "Numerical Characterization of  
406 Piezoceramics Using Resonance Curves." *Materials*, **9**(2), 71 (2016).
- 407 [19] Chillara, V. K., Ren, B., and Lissenden, C. J. "Guided wave mode selection for inhomogeneous elastic  
408 waveguides using frequency domain finite element approach." *Ultrasonics*, **67**, 199-211 (2016).
- 409 [20] Zhang, S., and Yu, F. "Piezoelectric materials for high temperature sensors" *Journal of the American  
410 Ceramic Society*, **94**(10), 3153-3170 (2011).
- 411 [21] COMSOL Multiphysics documentation, version 5.2. COMSOL AB, Stockholm, Sweden (2016)
- 412 [22] Rupitsch, S. J., and Ilg, J. "Complete characterization of piezoceramic materials by means of two block-  
413 shaped test samples" *IEEE Transactions on Ultrasonics, Ferroelectrics, and Frequency Control*, **62**(7),  
414 1403-1413 (2015).

- 415 [23] Ren, B., and Lissenden, C. J. "A fully coupled model for actuation of higher order modes of Lamb waves".  
416 In *AIP Conference Proceedings*, **1806**, 030009, AIP Publishing (2017).

ACCEPTED MANUSCRIPT

## Highlights:

- The effect of all ten temperature-dependent material coefficients is investigated numerically on both the radial and thickness mode resonances of a piezoelectric (PZT-5A) disc.
- The temperature dependent variation in  $s_{33}$  showed highest sensitivity towards the thickness resonance mode followed by  $\epsilon_{33}$ ,  $s_{11}$ ,  $s_{13}$ ,  $s_{12}$ ,  $d_{31}$ ,  $d_{33}$ ,  $s_{44}$ ,  $\epsilon_{11}$ , and  $d_{15}$  in the decreasing order of the sensitivity index.
- For radial resonance modes, the temperature dependence of  $\epsilon_{33}$  showed highest sensitivity index followed by  $s_{11}$ ,  $s_{12}$  and  $d_{31}$  coefficient.
- A complex interplay between various temperature-dependent piezoelectric coefficients causes the reduction of thickness mode resonance frequencies which is found to be in agreement with the experimental work.
- Proposed methodology based on the temperature dependent experimental data could potentially be used to estimate the sensitivity of piezoelectric based ultrasonic transducers at high temperatures.